

Comparative study of water dissociation on Rh(111) and Ni(111) studied with first principles calculations

Monica Pozzo

Department of Earth Sciences, University College London, Gower Street, London WC1E 6BT, United Kingdom

Gianluigi Carlini

Dipartimento di Fisica, Università degli Studi di Trieste, 34012 Trieste, Italy

Renzo Rosei

Dipartimento di Fisica, Università degli Studi di Trieste, 34012 Trieste, Italy and Laboratorio TASC, CNR, Area di Ricerca, Padriciano, 34012 Trieste, Italy

Dario Alfè

Department of Earth Sciences, University College London, Gower Street, London WC1E 6BT, United Kingdom; Department of Physics and Astronomy, University College London, Gower Street, London WC1E 6BT, United Kingdom; London Centre for Nanotechnology, University College London, Gower Street, London WC1E 6BT, United Kingdom; and INFN Democritos National Simulation Centre, 34104 Trieste, Italy

(Received 7 December 2006; accepted 22 February 2007; published online 24 April 2007)

The dissociation and formation of water on the Rh(111) and Ni(111) surfaces have been studied using density functional theory with generalized gradient approximation and ultrasoft pseudopotentials. Calculations have been performed on 2×2 surface unit cells, corresponding to coverages of 0.25 ML, with spot checks on 3×3 surface unit cells (0.11 ML). On both surfaces, the authors find that water adsorbs flat on top of a surface atom, with binding energies of 0.35 and 0.25 eV, respectively, on Rh(111) and Ni(111), and is free to rotate in the surface plane. Barriers of 0.92 and 0.89 eV have to be overcome to dissociate the molecule into OH and H on the Rh(111) and Ni(111) surfaces, respectively. Further barriers of 1.03 and 0.97 eV need to be overcome to dissociate OH into O and H. The barriers for the formation of the OH molecule from isolated adsorbed O and H are found to be 1.1 and 1.3 eV, and the barriers for the formation of the water molecule from isolated adsorbed OH and H are 0.82 and 1.05 eV on the two surfaces. These barriers are found to vary very little as coverage is changed from 0.25 to 0.11 ML. The authors have also studied the dissociation of OH in the presence of coadsorbed H or O. The presence of a coadsorbed H atom only weakly affects the energy barriers, but the effect of O is significant, changing the dissociation barrier from 1.03 to 1.37 and 1.15 eV at 0.25 or 0.11 ML coverage on the Rh(111) surface. Finally, the authors have studied the dissociation of water in the presence of one O atom on Rh(111), at 0.11 ML coverage, and the authors find a barrier of 0.56 eV to dissociate the molecule into OH+OH. © 2007 American Institute of Physics. [DOI: 10.1063/1.2717172]

I. INTRODUCTION

A molecular level understanding of the processes occurring on transition metal surfaces is crucial in order to improve our current knowledge on the heterogeneous catalytic reaction mechanisms. These are based upon the formation/dissociation of a molecule on a metal surface acting as a catalyst (e.g., by reducing the activation barrier of the occurring reaction). A typical catalytic reaction is the oxidation of H on a metal surface (i.e., O+H) which produces the adsorbate hydroxyl OH. This, in turn, can react with H (i.e., OH+H) to produce H₂O. Conversely, water may dissociate into OH, H, and O. Many important industrial catalytic processes (e.g., steam reforming, water gas shift, etc.) include the steps of water formation/dissociation. It is therefore vital to understand how water forms and interacts with the atoms on different metal surfaces of catalytic relevance.

Available literature about the interaction of water with solid surfaces is extensive both regarding different theoretic

cal approaches and experimental techniques, and we refer the reader to the exhaustive overviews of Thiel and Madey¹ and Henderson² (see also Ref. 3 and references therein). Michaelides⁴ has recently discussed density functional theory (DFT) studies regarding water-metal interfaces, pointing to ambiguities arising from experimental results due to the difficulties in disentangling the true water-metal interaction from water cluster formation. In general, heterogeneous catalysis studies motivated by industrial applications mainly focused on catalysts from the platinum group (such as Pt, Pd, Rh, and Ru) and their alloys. Hickman and Schmidt⁵ proposed a potential-energy diagram for the catalytic partial oxidation of methane CH₄ over Pt and Rh surfaces, producing mostly H₂ and CO. From their model, which is based on several experimental investigations, it emerged that on Rh surfaces, as opposed to Pt surfaces, the formation of water is lower due to a larger barrier for OH formation, while the production of H₂ is larger, making Rh more appealing as

catalyst for synthesis gas production from methane. However, Rh has the drawback of being the most expensive metal and therefore there is an urge to find an adequate alternative. Ni, above the Pt column in the Periodic Table, is the most natural choice. It has the catalytic ability of dissociating water into OH and H,³ and its hydroxide compounds (Ni–OH) are widely used (see Ref. 6 and references therein). Furthermore, Ni is a good catalyst not only for the dissociation of methane CH₄ (Ref. 7) and CO (Ref. 8) but also for hydrogen production through the catalytic steam reforming reaction of methane, CH₄+H₂O→CO+3H₂. However, natural gas must be saturated with steam in order to avoid excessive formation of carbon, which may lead to the catalyst deactivation. This implies the need for an additional water-gas shift reaction CO+H₂O→CO₂+H₂ to eliminate CO, for a net reaction CH₄+2H₂O→CO₂+4H₂, although this reduces the efficiency while increasing the cost of the overall process (alternative processes have been investigated, see, for example, Ref. 9 and references therein). Finally, Ni is appealing for possible hydrogen storage applications due to its ability to dissociate molecular hydrogen on an alloy surface to form a metallic interstitial hydride (see, for example, Refs. 10 and 11 for a review).

For these reasons we have decided to perform accurate DFT calculations in order to investigate the dissociation and formation of water on both Rh(111) and Ni(111) metal surfaces. There are just a few papers in literature about DFT studies of water on Rh(111) (Refs. 12–15) and on Ni(111) (Ref. 3) metal surfaces. About water dissociation products, the interaction of H on metal surfaces was studied and reviewed by Christmann.¹⁶ Specifically, experimental results for H on Rh(111) surfaces are referenced by Greeley and Mavrikakis,¹⁷ while theoretical results obtained using *ab initio* first principles approaches are presented by Wilke *et al.*,¹² Greeley and Mavrikakis,¹⁷ and Mavrikakis *et al.*¹⁸ Regarding H on Ni(111), despite the large number of available papers reporting experimental studies spanning some 40 years (see Ref. 17 and references therein), surprisingly there are just a few first principles theoretical papers.^{17,19–22} Available theoretical literature for both Rh(111) and Ni(111) surfaces regarding the other water dissociation products (O, OH) is even sparser,^{3,4,12,18,19,23} while several experimental studies have been reported (see, for example, Refs. 25–27; see also Refs. 6, 18, and 24 and references therein).

Nonetheless, it is striking that in none of all the above listed theoretical papers a fully consistent investigation with DFT on both water and its dissociation products (H, O, OH) on Rh and Ni has ever been presented [apart from a study of water formation on Rh (Ref. 12)]. This has motivated our comparison study on both Rh(111) and Ni(111) surfaces.

The paper is organized as follows. Details about first principles DFT calculations are described in Sec. II. In Sec. III we present the results obtained for Rh(111) and Ni(111) clean surfaces, for (O₂, H₂, OH, and H₂O) isolated molecules in the gas phase and also for the adsorption of O, H, OH, and H₂O on both metal surfaces. Activation energies for O, H, and OH diffusion on Rh and Ni are also given, together with

a study of the dissociation/formation mechanisms of OH and H₂O. It follows a discussion on the energy diagrams for these reactions on Rh(111) and Ni(111). Finally, conclusions are summarized in Sec. IV.

II. TECHNICAL DETAILS

Calculations have been performed using DFT with the generalized gradient approximation (GGA) of Perdew, Burke, and Ernzerhof known as PBE.²⁸ The ionic cores have been described using ultrasoft pseudopotentials²⁹ (USPPs) and single particle orbitals expanded in plane waves with a plane-wave cutoff of 30 Ry and a cutoff for the charge density of 240 Ry. The code used for the calculations was PWSCF.³⁰ Figures 1–5 have been made using XCRYSDEN software.³¹

Surfaces have been modeled using slab geometry, with three atomic layers and a vacuum region of 12 Å. Two atomic layers have been fixed to the bulk interatomic distance and only the third atomic layer has been allowed to relax. Tests performed with four atomic layers, two of which were allowed to relax, did not show significant differences in total energies and structural parameters. Convergence with respect to the thickness of the vacuum region has also been carefully tested.

Calculations have been performed on 2×2 (corresponding to 0.25 ML coverage) and checked against results obtained from 3×3 (corresponding to 0.11 ML coverage) surface unit cells. Integration inside the Brillouin zone (BZ) has been performed by summation over 15 surface Monkhorst-Pack (MP) special points for the 2×2 unit cell and the correspondingly equivalent 6 points for the 3×3 unit cell. The 15 points are obtained using a shifted 3×3×1 MP grid, while the 6 points are obtained using a shifted 2×2×1 MP grid. These choices allow an equivalent BZ sampling in the 2×2 and 3×3 surface unit cells. A smearing function of Methfessel-Paxton³² (product of a Gaussian times a first order Hermite polynomial) and width=0.13 eV has been used throughout.

Activation energies have been calculated using the nudged elastic band (NEB) method, which allows the determination of the closest minimum energy path (MEP) between two prespecified configurations of energy minima. This is done by introducing a number of “images” of the system distributed along the MEP. Initially, these images may be guessed by a simple linear interpolation between the initial and the final states. The method then consists in relaxing the position of each image in the direction perpendicular to the path connecting the images. Springs between the images are introduced in order to allow movement also in the direction parallel to the path, but preventing the collapsing of all the intermediate images onto the initial or the final state. A refinement of the method called “climbing image” also allows the image with the highest energy to climb to the saddle point, which therefore permits an accurate determination of the transition state. A sufficient number of images has to be used in order to predict accurately the MEP. For most cases we repeated the calculations with a different number of

TABLE I. Equilibrium lattice constant (a_0), bulk modulus (B), magnetic moment (M), and relaxation of the first layer for Rh(111) and Ni(111) compared to previous theoretical calculations and corresponding experimental values.

Surface	a_0 (Å)	B (GPa)	M (μ_B)	Δd_{12} (%)
Rh(111) [Expt.]	3.86, ^a 3.83 ^{b-d} [3.80] ^e	258, ^a 259 ^b [270] ^f		-2.6(-0.2) ^g
Ni(111) [Expt.]	3.52, ^a 3.52 ^g [3.52] ^e	201, ^a 194 ^g [186] ^f	0.63, ^a 0.61, ^g 0.69 ^h [0.61] ^f	-1.7, ^a -1.3, ^g -0.9 ⁱ [<2] ^j

^aThis work. “+” refers to the relaxation value given in parentheses obtained using a lattice constant of 3.81 Å instead of 3.86 Å.

^bReference 23 (from FP-LAPW GGA-PW91 calculations).

^cReference 18 (from USPP GGA-PW91 calculations).

^dReference 13 (from USPP GGA-PW91 calculations).

^eReference 35.

^fReference 36.

^gReference 21 (from PAW GGA-PW91 calculations using a four-layer slab).

^hReference 17 (from USPP GGA-PW91 calculations).

ⁱReference 37 (from local-spin-density-functional calculations using a nine-layer slab).

^jReference 38.

images, obtaining essentially identical results in each case. The total number of images actually used in each case is reported where relevant in the following sections. For a detailed technical explanation of the NEB method see Ref. 33.

III. RESULTS

A. Bulk Rh and the Rh(111) clean surface

To obtain the lattice constant of bulk Rh we fitted a Birch-Murnaghan³⁴ equation of state to a set of energies calculated at a number of different volumes. We obtained a lattice constant of 3.86 Å, which is 1.5% larger than the experimental value of 3.80 Å (Ref. 35) and somewhat larger than what is found from previous DFT calculations (see Table I and references therein). This difference may be of significance, and for this reason we have repeated some of the calculations (to be presented later in the paper) both using the calculated value of 3.86 Å and the value of 3.81 Å, close to the experimental value. Results show that adsorption energies and energy barriers do not change significantly when one or the other lattice parameters are used (see below). The calculated bulk modulus of 258 GPa is about 4% lower than the experimental value of 270 GPa but in agreement with values reported from other DFT calculations (see Table I). On the clean (111) surface the topmost layer has an inward relaxation of -2.6%.

B. Bulk Ni and the Ni(111) clean surface

The calculated lattice constant for bulk Ni is 3.52 Å, which is (possibly accidentally) in perfect agreement with the experimental value of 3.52 Å.³⁵ The calculated bulk modulus is 201 GPa, about 8% higher than the experimental value (see Table I). Bulk Ni is ferromagnetic. Our calculations predict a magnetic moment of 0.63 μ_B , in good agreement with the experimental value and previous DFT calculations (see Table I). On our clean (111) surface the topmost layer has an inward relaxation of -1.7%, which is consistent

TABLE II. Interatomic distance ($d_{\text{atom-atom}}$) and binding energy (E_{bind}) of isolated molecules in the gas phase.

Molecules	$d_{\text{atom-atom}}$ (Å)	E_{bind} (eV)
O ₂ [Expt.]	1.24 ^a [1.21] ^c	6.58, ^a 6.20/6.24 ^b [5.18] ^c
H ₂ [Expt.]	0.75 ^a [0.74] ^c	4.54, ^a 4.55/4.55, ^b 4.56/4.54 ^d [4.48] ^{+,c} [4.73] ^f
OH [Expt.]	0.99 ^a [0.97] ^g	4.81, ^a 4.77/4.77 ^b [4.63] ^g
H ₂ O [Expt.]	0.97 ^a [0.96] ^c	10.32, ^a 10.19/10.15, ^b 10.30/10.26 ^d [10.06] ^f

^aThis work.

^bReference 28 (from GGA-PW91/PBE calculations).

^cReference 35.

^dReference 41 (from GGA-PW91/PBE calculations).

^eReference 39. “+” refers to the experimental values that includes zero point motion, which for the hydrogen molecule reduces the binding energy by 0.27 eV.

^fReference 42 (excluding zero point motions).

^gReference 40.

with <2% experimental deviation found by Lu *et al.*³⁸ but somewhat larger than values found from other theoretical calculations (see Table I).

C. O₂, H₂, OH, and H₂O molecules in the gas phase

Structural parameters and binding energies for isolated molecules have been obtained by performing calculations in large periodically repeated cubic boxes, with sides larger than 15 Å. We carefully checked convergence of the results with respect to the size and the shape of the periodically repeated box. No zero point motion has been included in the present calculations. Results are presented in Table II and compared with corresponding experimental values and previous theoretical calculations.

The isolated O₂ molecule (the only elementary molecule in this study to carry a permanent magnetic moment) has a positive magnetic moment equal to 2.0 μ_B . The internuclear distance is 1.24 Å, and the binding energy is 6.58 eV, which are somewhat larger than the experimental values (see Table II).

The internuclear distance of the H₂ molecule is found to be 0.75 Å, and the binding energy is 4.54 eV which compares well with the experimental values (see Table II).

The internuclear distance of the OH molecule is calculated to be 0.99 Å and the binding energy is 4.81 eV, close to the experimental and previous DFT values reported in Table II.

The HOH angle of the water molecule and the OH distance are calculated to be 104.6° and 0.97 Å, respectively. These compare well with the corresponding experimental values.^{35,43} Such good agreement between theory and experiments is typical of DFT-GGA calculations.^{13,44} The binding energy of the water molecule is instead calculated to be 10.32 eV, somewhat larger than previously reported experimental and theoretical values (see Table II). We should point out that previous DFT calculations of binding energies^{17,41}

TABLE III. Binding energies E_{bind} of O, H, OH, and H₂O on Rh(111) (1/4 ML coverage) in various adsorption sites, calculated using a 2×2 unit cell, defined as $E_{\text{bind}}(X) = E_{X/\text{Rh-slab}} - E_{\text{Rh-slab}} - E(X)$, where $E_{X/\text{Rh-slab}}$ is the energy of the slab covered with species X, $E_{\text{Rh-slab}}$ the energy of the clean slab, and $E(X)$ the energy of species X in the gas phase, with X=O, H, OH, or H₂O.

Adsorption site	E_{bind} (eV)				
	O	H	OH	H ₂ O	
fcc	5.06, ^a 5.51, ^b 4.88 ^c	2.79, ^a 2.82, ^b 2.79, ^c 2.81 ^d	2.92, ^a 3.34, ^b 2.89 ^c	0.11, ^a 0.00, ^b 0.12 ^e	
hcp	5.03, ^a 5.42, ^b 4.85 ^c	2.76, ^a 2.78, ^b 2.75, ^c 2.80 ^d	... ^a 3.17, ^b 2.74 ^c	0.11, ^a ... ^b	
Top	3.65, ^a ... ^b 3.58 ^c	2.50, ^a 2.38, ^b 2.57 ^c	2.09, ^a ... ^b 2.09 ^c	0.35, ^a 0.35, ^b 0.41, ^c 0.42 ^f	
Bridge	4.60, ^a 4.86, ^b 4.43 ^c	2.67, ^a 2.64, ^b 2.68 ^c	2.97- ^a 3.04, ^b 2.68 ^c	... ^a 0.22, ^b 0.13 ^e	
Activation energy for diffusion	0.46, ^a 0.65, ^b 0.45 ^c	0.12, ^a 0.17, ^b 0.10, ^c 0.11 ^d	0.26 ^a		

^aThis work. In the bridge site the molecule is tilted (denoted by “-”), with the O atom at the bottom shifted towards the fcc site and the H atom towards the hcp site. Accurate convergence tests show that hcp for OH and bridge for H₂O are unstable, leading to a tilted bridge and a top site, respectively.

^bReference 12 (from FP-LAPW GGA-PW91 calculations using a five-layer slab).

^cReference 18 (from USPP-GGA-PW91 calculations using a three-layer slab).

^dReference 17 (from USPP GGA-PW91 calculations using a four-layer slab).

^eReference 13 (from USPP GGA-PW91 calculations using a 3×3 unit cell and a four-layer slab).

^fReference 14 (from USPP GGA-PW91 calculations using a five-layer slab).

have shown a tendency for GGA-PW91 DFT calculations to overestimate the binding energies with respect to the other functionals. However, they turn out to be into a better agreement with the experimental values once zero point energy corrections are included.

D. Adsorption of O, H, OH, and H₂O on Rh(111)

Adsorption of the O and H atoms and the OH and H₂O molecules on the Rh(111) surface has been studied using a 2×2 unit cell with a lattice parameter of 3.81 Å. Some of the calculations have also been repeated using a 3×3 unit cell and/or the GGA calculated lattice parameter of 3.86 Å, with no significant differences in the calculated relevant quantities. We report these results in Sec. III J.

In Table III we list the adsorption energies for the O and H atoms and the OH and H₂O molecules in different adsorption sites compared with experimental and other theoretical values. In Table IV we report the perpendicular distances of O, H, OH, and H₂O adsorbates to the plane of nearest-neighbor surface metal atoms. We also report the OH bond lengths for OH and H₂O and the H–O–H angle.

For both O and H we find that the preferred adsorption site is the threefold fcc, with binding energies of 5.06 and 2.79 eV, respectively. In agreement with previous theoretical calculations, we find that the difference in energy between the most stable fcc site and the next most stable hcp site is only 0.03 eV. Mavrikakis *et al.*¹⁸ showed that zero point effects are unlikely to alter these site preferences. The distance between the oxygen atom and the plane formed by the three surrounding Rh atoms is 1.31 Å. The corresponding experimental value is of 1.25 ± 0.05 Å, which covers the range of values found from other DFT studies (see Table IV). These

three Rh atoms which form the fcc adsorption site have a slight outward relaxation, opposed to the Rh atom with no O neighbors which has a slight inward relaxation, consistent with experimental findings.⁴⁵ The distance between the hydrogen atom and the plane formed by the three surrounding Rh atoms is 0.99 Å, also consistent with previous DFT calculations (see Table IV and references therein).

The OH molecule adsorbs with the axis of the molecule tilted over a bridge between the fcc and the hcp sites, with a binding energy of 2.97 eV (see Table III). The next most stable site is the fcc, with a binding energy 0.05 eV lower (2.92 eV). In this site we found that the molecule is almost free to tilt. The distance between the O atom and the plane is 1.69 Å, consistent with previous DFT calculations (see Table IV). The O–H distance for the adsorbed molecule in our bridge site is 0.98 Å. Isolated O and H atoms on the surface have a binding energy which is only 0.07 eV lower than that of the adsorbed OH molecule, which is therefore only slightly less stable than its dissociation products.

The water molecule adsorbs flat on the surface, with the oxygen atom binding on top a rhodium atom, at a distance of 2.30 Å. This distance is larger than that of the hydroxyl group on the same site (see Table IV), which is a signal of a weaker bond between the molecule and the surface. The HOH angle of the adsorbed molecule in this site is 104.9°, and the O–H distance is 0.98 Å, not very different from the values found with the molecule in the gas phase, and further confirming that the interaction between the molecule and the surface is weak. We found the binding energy to be the same if the molecule was rotated by 90° around an axis perpendicular to the plane of the surface, in agreement with Wilke *et al.*,¹² which indicates that the molecule is free to rotate on the surface. The calculated value of the binding energy is

TABLE IV. Perpendicular distances of A=O, H, OH, and H₂O adsorbates to the plane of nearest-neighbor surface metal atoms. Also given there are the OH bond lengths ($d_{\text{O-H}}$) for OH and H₂O and the H–O–H angle (α_{HOH}).

A surface	O		OH		H ₂ O		α_{HOH}
	$d_{\text{A-surf}}$ (Å)	$d_{\text{A-surf}}$ (Å)	$d_{\text{A-surf}}$ (Å)	$d_{\text{O-H}}$ (Å)	$d_{\text{A-surf}}$ (Å)	$d_{\text{O-H}}$ (Å)	
Rh(111)	1.31, ^a 1.21, ^b	0.99, ^a	1.69 ^{*,a}	0.98 ^{*,a}	2.30, ^a	0.98, ^a	104.9, ^a
	1.23, ^c 1.24 ^d	0.98, ^c 0.96 ^e	1.53 ^{+,b}	0.98 ^{++c}	2.32, ^f	0.98, ^f	105.9, ^f
			1.51 ^{++c}		2.31 ^g	0.98, ^g	106 ^g
[Expt.]	[1.25±0.05] ⁱ					[0.96] ^h	[104.5] ^h
Ni(111)	1.13, ^a 1.19 ^j	0.91, ^a 0.89, ^k	1.51, ^a	0.98 ^a	2.24, ^a	0.98 ^a	104.8 ^a
		0.90, ^c 1.20 ^j	1.51 ^j		2.06 ^l		
[Expt.]	[1.14] ^m	[0.98±0.08] ⁿ				[0.96] ^h	[104.5] ^h

^aThis work. “*” refers to values found for the most favorable tilted bridge site.

^bReference 12 (from FP-LAPW GGA-PW91 calculation using a five-layer slab). “+” refers to the value for their (most favorable) fcc site.

^cReference 18 (from USPP GGA-PW91 calculations using a three-layer slab). “++” refers to the reported values for their (most favorable) fcc site. Note that a value of 1.6 Å is instead reported for the O distance to the plane for the tilted bridge site.

^dReference 23 (from FP-LAPW GGA-PW91 calculations using a seven-layer slab).

^eReference 17 (from USPP GGA-PW91 calculations using a four-layer slab).

^fReference 13 (from USPP GGA-PW91 calculations using a four-layer slab).

^gReference 14 (from USPP GGA-PW91 calculations using a five-layer slab).

^hThe reported values are for the free water molecule (Ref. 43).

ⁱReference 45.

^jReference 24 (from *ab initio* embedding theory and configuration interaction calculations using a three-layer, 62-atom cluster).

^kReference 20 (from GGA-PBE calculations using a four-layer slab).

^lReference 3 (from *ab initio* embedding theory and configuration interaction calculations using a three-layer, 62-atom cluster).

^mReference 46.

ⁿReference 47.

0.35 eV. This is less than half of the experimental value of 0.74 eV,⁴⁸ but in good agreement with other theoretical results (see Table III and references therein). This low value for the binding energy of the molecule is also the reason why the internal geometry of the molecule is hardly affected by adsorption on the rhodium surface. A second minimum also exists with the molecule still flat on the surface and the oxygen atom in the fcc site. The binding energy in this configuration is 0.11 eV and the molecule sits at a much larger distance from the first surface layer of 3.12 Å. The hcp site is equally favorable. At variance with Wilke *et al.*,¹² we found that the bridge site is not stable. However, we also found that the potential energy surface is quite flat in the vicinity of this site, with only small forces carrying away the molecule towards the top site. The binding energies of one O and two H atoms on the surface is essentially the same as that of the adsorbed molecule, which is therefore as stable as its dissociation products. Michaelides *et al.*¹⁴ have shown that the water molecule is more strongly bounded on Rh(111) than on other metal surfaces, although they also found low adsorption energies (0.1–0.4 eV only), implying weak water-metal bonds. It should be noted that DFT with the current implementations of exchange-correlation functionals cannot properly describe van der Waals forces, which could cause some uncertainty in calculating binding energies and might also alter site preference for weakly adsorbed molecules.

E. Adsorption of O, H, OH, and H₂O on Ni(111)

Adsorption of the O and H atoms and the OH and H₂O molecules on the Ni(111) surface has been studied using a 2 × 2 unit cell and the calculated lattice parameter of 3.52 Å.

In Table V we list the adsorption energies for the O and H atoms and the OH and H₂O molecules in different adsorption sites, together with the results from previous theoretical studies.

For both O and H the preferred adsorption site is the threefold fcc. We find a binding energy of 5.50 eV for O. For H in the fcc site we find a binding energy of 2.78 eV, in good agreement with the experimental value of 2.75 eV,⁵⁰ but we note that the hcp site is competing with an energy difference of just 0.01 eV. The distance between the oxygen atom and the plane formed by the three surrounding Ni atoms is 1.13 Å, in very good agreement with the experimental value (see Table IV). The three Ni atoms which form the fcc adsorption site have a slight outward relaxation, opposed to the Ni atom with no O neighbors, which has a slight inward relaxation, in agreement with experimental results.⁴⁶ The distance between the hydrogen atom and the plane formed by the three surrounding Ni atoms is 0.91 Å, in fair agreement with the experimental value of 0.98±0.08 Å (Ref. 47) and previous DFT calculations (see Table IV and references

TABLE V. Binding energies E_{bind} of O, H, OH, and H₂O on Ni(111) in various adsorption sites, calculated using a 2×2 unit cell. The binding energies are defined similarly to those in Table III.

Adsorption site	ΔE_{bind} (eV)			
	O	H	OH	H ₂ O
fcc	5.50, ^a 3.99 ^b	2.78, ^a 2.69, ^b 2.91, ^c 2.60, ^d 2.87, ^e 2.89 ^f	3.14, ^a 3.90 ^b	0.11, ^a 0.35 ^g
hcp	5.41 ^a	2.77, ^a 2.69, ^b 2.91, ^c 2.54, ^d 2.86, ^e 2.88 ^f	3.08, ^a 3.90 ^b	0.11, ^a 0.25 ^g
Top	3.69, ^a 1.99 ^b	2.21, ^a 2.34, ^b 2.08, ^c 2.27 ^e	... ^a 3.21 ^b	0.25, ^a 0.50 ^g
Bridge	4.96, ^a 3.21 ^b	2.64, ^a 2.56, ^b 2.73, ^c 2.73 ^e	3.03, ^a 3.69 ^b	0.13, ^a 0.31 ^g
Activation energy for diffusion	0.54 ^a	0.14, ^a 0.14 ^f	0.24 ^a	

^aThis work. As for Rh(111), in the bridge site the molecule is tilted, with the O atom at the bottom shifted towards the fcc site and the H atom shifted towards the hcp site.

^bReference 24 (from *ab initio* embedding theory and configuration interaction calculations using a three-layer, 62-atom cluster).

^cReference 20 (from GGA-PBE calculations using a four-layer slab).

^dReference 22 [using nonlocal pseudopotentials of Lin *et al.* (Ref. 49) and a three-layer slab].

^eReference 21 (from PAW GGA-PW91 calculations using a four-layer slab). Note that we have converted their binding energy values to our scale which is defined with respect to the energy of the atomic H and O rather than H₂ and O₂.

^fReference 17 (from USPP GGA-PW91 calculations and a four-layer slab).

^gReference 3 (from *ab initio* embedding theory and configuration interaction using a three-layer, 62-atom cluster).

therein). The presence of adsorbed H induces the same type of relaxation as oxygen, consistent with the experimentally observed behavior.⁴⁷

The OH molecule adsorbs in the fcc site with the axis of the molecule perpendicular to the surface, with a binding energy of 3.14 eV [slightly larger than 2.97 eV of the Rh(111) surface, see Tables III and V]. At variance with Yang and Whitten,²⁴ we find the top site to be unstable, and we found a stable bridge site in which the molecule is tilted in a similar way than on Rh(111). However, at variance with the Rh(111) case where this tilted bridge site is the lowest in energy, on Ni(111) the OH molecule adsorbed in this tilted bridge site has an adsorption energy which is 0.11 eV lower (3.03 eV). The distance between the O atom and the plane is 1.51 Å and the O–H distance for the adsorbed molecule in our fcc site is 0.98 Å. Isolated O and H atoms on our Ni surface have a binding energy which is 0.33 eV lower than that of the adsorbed OH molecule, which therefore has a significant thermodynamic advantage to dissociate.

Similarly to the Rh(111) surface, the water molecule adsorbs flat on the surface, with the oxygen atom sitting on top a nickel atom at a distance of 2.24 Å and with a binding energy of 0.25 eV (see Tables IV and V, respectively). The HOH angle of the adsorbed molecule is 104.8°, and the O–H distance is 0.98 Å, similar to the values found for Rh and to those known for the molecule in the gas phase, confirming that the interaction between the molecule and the Ni surface is weak too. Also on this surface the molecule is free to rotate around an axis perpendicular to the surface. Yang and Whitten³ found the same preferred site for molecular water but report a binding energy of 0.50 eV. They found that the

molecule is tilted by about 25° from the surface normal, although tilting the molecular plane from 0° to 50° or rotating the molecule by 90° around the surface normal does not change the energy substantially, in agreement with the random distribution observed experimentally.⁵¹ Their value for the binding energy is twice the value we find and may be due to their many-electron embedding theory approach as opposed to our DFT calculations, which is known to have difficulties in accurately predicting such low adsorption energies. Their result seems to be in better agreement with the experimental value of 0.43 eV (Ref. 52) found from thermal desorption data (TPD) for first layer chemisorbed water, although a word of caution here is in order, as adsorption energies obtained by TPD experiments often rely on some guessed value for the prefactor (typically 10¹³ s⁻¹) which may be orders of magnitudes different from the correct value (see Ref. 53). Our calculated value of 0.25 eV for the atop binding energy is somewhat lower than the 0.35 eV binding energy on the Rh(111) surface. The binding energies of one O and two H atoms on the surface are 0.49 eV lower than that of the adsorbed molecule. The increased stability of the dissociation products with respect to the adsorbed molecule on the nickel surface is due to the increased binding energy of the oxygen atom, which is almost 0.5 eV higher on Ni(111) than on Rh(111).

F. Activation energies for O, H, and OH diffusion on Rh(111) and Ni(111) surfaces

Activation energies and MEPs have been calculated using the NEB method. For the diffusion of O and H on the

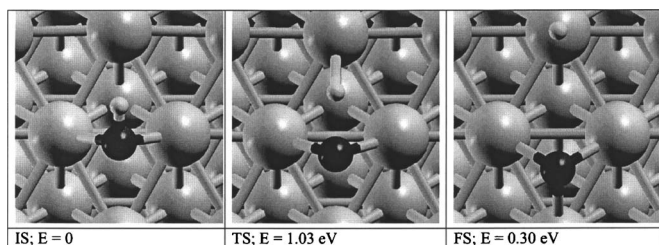


FIG. 1. Initial state (IS), transition state (TS), and final state (FS) of one possible MEP for the $\text{OH} \rightarrow \text{O} + \text{H}$ reaction on Rh(111). NEB calculations were performed using five images.

surface the MEP is straightforward, connecting the fcc and the hcp adsorption sites through the bridge site. In fact, in this particular case, we found that the transition state (the state with the maximum energy in the MEP) coincides with the bridge adsorption site for both O and H, so that activation energies are simply given by the difference in energies between the bridge and the fcc or the hcp sites. Calculations using the 2×2 unit cell give 0.46 (0.54) and 0.12(0.14) eV for O and H, respectively, on the Rh(111) (Ni(111)) surface. These values are also reported in Table III and V, together with previous theoretical results.

For the diffusion of OH the MEP on Ni(111) is similar to the previous two, with the initial and final states located on the fcc and hcp sites, respectively, and transition state located on the bridge site, although at variance with O and H the bridge site is not a stable site (note: not the *tilted* bridge site, which is instead a stable site, though with an adsorption energy 0.11 eV higher than the most stable fcc site). The energy barrier on Ni(111) is 0.24 eV. On Rh(111) the initial and final states were two nearby tilted bridge sites, with the MEP going through a hcp site. The transition state is located near the bridge site, and the energy barrier is found to be 0.26 eV. These calculations have been performed using seven images along the reaction path.

Experimental values of 0.58 eV (Ref. 54) and 0.14 eV (Ref. 55) have been reported, respectively, for the diffusion activation energy of O (at 0.25 ML coverage) and H (at 0.3 ML coverage) on Rh(111). Experimental values of 0.10–0.20 eV (Ref. 56) have been reported for the surface diffusion barrier of H on Ni(111).

G. OH dissociation/formation on Rh(111)

Given that the preferred adsorption site of the OH molecule on Rh(111) is “across” the bridge, one possible final state would be O and H in two neighboring fcc and hcp sites, with the molecule breaking on the bridge site and the two atoms falling in the two neighboring sites. However, we found that this state is not stable, and the H atom is pushed from the hcp to the next top site. We therefore considered this as one possible final state. In Fig. 1 we display the initial (IS), transition (TS), and final (FS) states for the minimum energy path calculated using a 2×2 unit cell and five images in the NEB method. The activation energy for the dissociation of the molecule is equal to 1.03 eV, significantly higher than the values of 0.22 and 0.30 eV reported, respectively, by Zum Mallen *et al.*²⁷ and Wilke *et al.*¹²

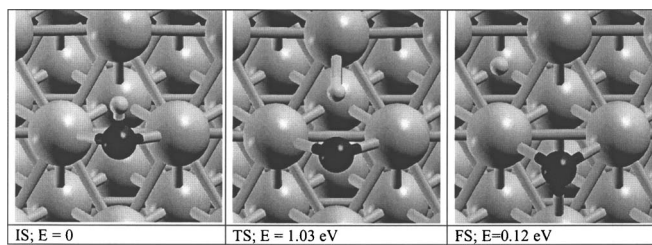


FIG. 2. As in Fig. 1 but for a second possible MEP for the $\text{OH} \rightarrow \text{O} + \text{H}$ reaction. NEB calculations were performed using five and ten images.

The activation energy for the formation of the molecule, i.e., the inverse barrier, is determined by the difference between the binding energies of the isolated atoms and that of the transition state and is equal to 1.10 eV. This large energy barrier value for OH (and therefore water) formation on the Rh surface makes Rh a superior catalyst than Pt for the partial catalytic oxidation of methane (see Ref. 5).

A second possibility to consider is a final state in which O and H are in two next neighbor fcc sites. Details of the IS, TS, and FS are displayed in Fig. 2. NEB calculations have been performed with five and ten images, both giving essentially identical results. It is evident from the figure that the transition state is the same as the previous one, even though the final states are different. As a result, the activation energy for the dissociation and the formation of the molecule are exactly the same as those found for the previous path. Note, however, that the inverse barrier is *not* given by the energy difference between the transition state and the final state, but by the difference between the energy of the transition state and that of the dissociation products at infinite distance.

A third calculation has been performed with the IS in the fcc site, which is only 0.05 eV less stable than the bridge site, and the FS the same as that of the previous calculation. We used 5, 9, and 14 images for this calculation, all giving the same results for the transition state, which is found to be identical to the previous one. In fact, the calculations with the largest number of images also show that the path goes through the same bridge site discussed above.

Since adsorbed OH molecules are the dissociation products of H_2O molecules, we have repeated the study of the dissociation of OH in the presence of coadsorbed H or O atoms. The initial, transition, and final states of the MEP are displayed in Fig. 3. NEB calculations were performed using seven images. We found that the dissociation barriers in this case are 1.11 and 1.37 eV with coadsorbed H and O, respectively. As expected, the dissociation barriers (and the energy of the final state, which is usually linked to it) increase because the presence of the coadsorbates lowers the activity of the surface. This effect is only marginal for coadsorbed H but is significant for coadsorbed O. This is expected as O adsorption has a much stronger effect than H on the reactivity of transition metal surfaces. Notice also that the MEP is quite different in the case of coadsorbed H or O atoms. In the first case the path goes “near” the coadsorbed H atom, but in the second case it is repelled by the O atom, consistent with what is observed above about O and H not being able to be adsorbed in nearby hollow sites.

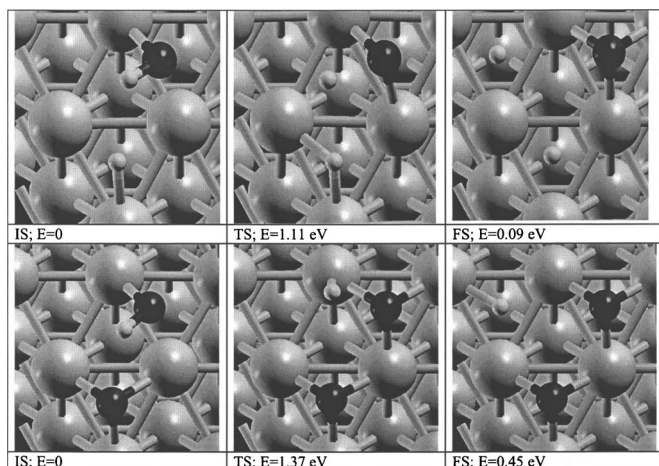


FIG. 3. As in Fig. 2 but in the presence of a coadsorbed H atom (top panels) or O atom (bottom panels) as “spectators.” NEB calculations were performed using seven images.

H. H₂O dissociation/formation on Rh(111)

To study water dissociation/formation we have analyzed a number of MEPs, starting with the water molecule in its ground state position on the on-top site. One possible path is depicted in Fig. 4. The activation energy for the dissociation of the molecule along this path ($\text{H}_2\text{O} \rightarrow \text{OH} + \text{H}$) is calculated to be 0.92 eV, which is much higher than 0.17 eV estimated by Wilke *et al.*¹² but significantly lower than the experimental value of 1.6 eV reported by Zum Mallen *et al.*²⁷ The activation energy for the formation of the water molecule is obtained by subtracting the energy of the isolated adsorbate products, OH_a and H_a , from that of the TS, which amounts to 0.82 eV.

In the presence of an adsorbed O atom, a second possibility for the dissociation of the water molecule is through the reaction $\text{H}_2\text{O} + \text{O} \rightarrow \text{OH} + \text{OH}$. It is interesting to analyze the MEP for this reaction, which is depicted in Fig. 5. The calculations have been performed using seven images and the 3×3 surface unit cell only, in order to avoid unwanted effect caused by periodic images. The pictures have been zoomed out compared with the previous ones, in order to facilitate the identification of the simulation cell. Our initial state corresponds to an adsorbed H_2O molecule and an adsorbed O atom in a nearby fcc site. As the oxygen atom moves towards the molecule along the MEP, one of the H atoms of the water molecule detaches from the molecule and is drawn closer to the O atom, until a OH radical is formed. In the breaking of the water molecule and the formation of

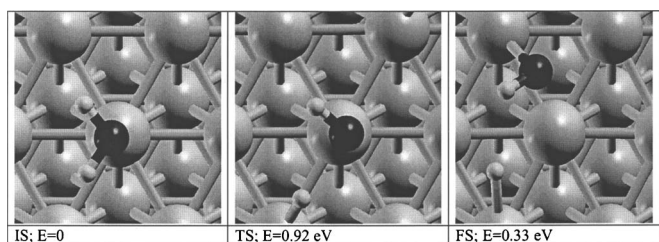


FIG. 4. IS, TS, and FS for the reaction $\text{H}_2\text{O} \rightarrow \text{OH} + \text{H}$ on Rh(111). NEB calculations were repeated with five and seven images.

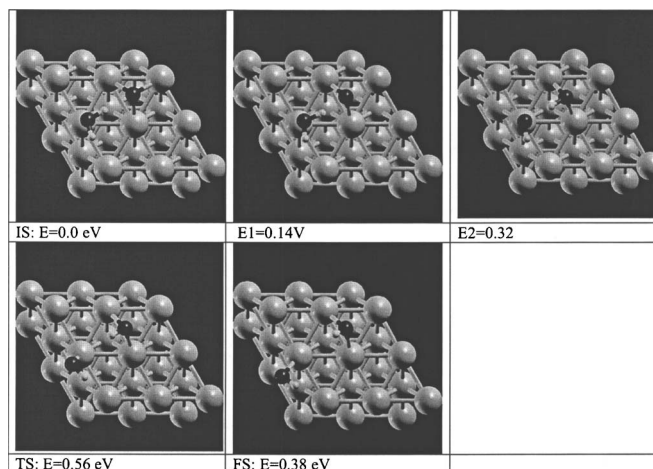


FIG. 5. Snapshots of the MEP for the reaction $\text{H}_2\text{O} + \text{O} \rightarrow \text{OH} + \text{OH}$ on Rh(111) (see text for details). Calculations were performed on a 3×3 surface unit cell using seven images.

the OH radical the proton only has to travel a very short distance, and no transition state is observed for this reaction. A transition state only appears when the formation of a second OH molecule is complete, after which both molecules are free to drift to their equilibrium positions. Figure 5 shows respectively the IS, the image corresponding to the configuration just before the breaking of the H_2O molecule (E1), the image corresponding to the configuration just after the two OH radical are formed (E2), the TS, and the FS. The maximum energy barrier for the whole process is only 0.56 eV, much lower than the 0.92 eV found for the previous reaction and significantly lower than 2.73 eV reported by Hickman and Schmidt.⁵ We show in Fig. 6 the energy profile corresponding to this MEP.

I. OH and H₂O dissociation/formation on Ni(111)

We repeated similar MEP calculations for the dissociation/formation of OH and H_2O on Ni(111), as previously done for the molecules on the Rh(111) surface (using a

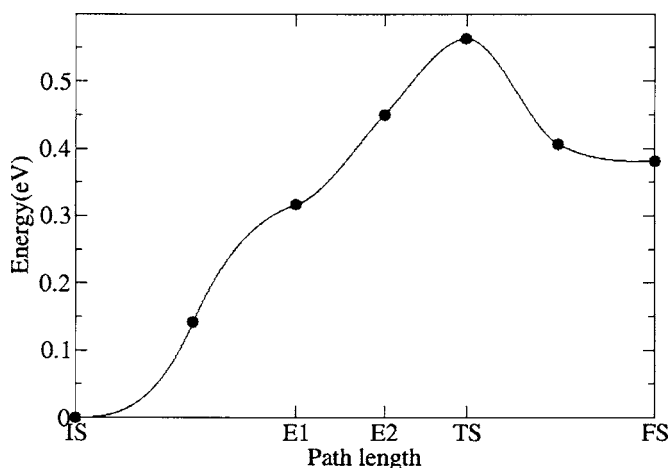


FIG. 6. Energy profile corresponding to the MEP for the reaction $\text{H}_2\text{O} + \text{O} \rightarrow \text{OH} + \text{OH}$ on Rh(111). IS is the initial state, E1 and E2 label the configurations before and after the transfer of a proton from the H_2O molecule to the O atom to form $\text{OH} + \text{OH}$, and TS is the transition state and FS the final state.

TABLE VI. Binding energies E_{bind} of H, O, OH, and H₂O on Rh(111) in various adsorption sites. Results have been obtained using a 3×3 unit cell and a lattice parameter for bulk rhodium of 3.81 Å. Also reported in parentheses are results obtained with a lattice parameter of 3.86 Å.

Adsorption site	E_{bind} (eV)			
	H	O	OH	H ₂ O
fcc	2.79 (2.82)	5.11 (5.12)		
hcp		5.04 (5.08)		
Top				0.38
Bridge	2.68 (2.70)	4.63 (4.66)	2.98	
Activation energy for diffusion	0.11 (0.12)	0.48 (0.47)		

2×2 unit cell). We note that despite Ni has only a small magnetic moment, the magnetic character of Ni cannot be ignored. In fact, as shown later in Table VI (values in parentheses) the results for the energy barrier for the reaction $\text{H}_2\text{O}_a \rightarrow \text{OH}_a + \text{H}_a$ calculated using non-spin polarized calculations are smaller by almost 0.2 eV.

For the dissociation of OH we considered two possible initial states: the first with the molecule in the most stable fcc site and the second with the molecule in the less stable tilted bridge site. The calculations were performed using five images, and the IS, TS, and FS of these two MEPS are shown in Fig. 7, where it is clear that the TS and the FS are the same in the two cases. We find the values 0.97 and 0.86 eV for the activation energies to dissociate OH in the two cases, respectively. This values are slightly lower than the one we found for the Rh(111) surface (1.03 eV), which implies that OH dissociate slightly more easily on Ni than on Rh surfaces. The inverse barrier for the formation of the OH molecule is instead of 1.3 eV, which is 0.2 eV higher than the corresponding value we found on Rh.

We have also performed the calculations in the presence of coadsorbed H and O atoms, at 0.25 ML coverage, and found that the dissociation barriers are changed from 0.97 to 1.06 eV and 1.19 eV, respectively. All these calculations have been performed using seven images, and the IS, TS, and FS are shown in Fig. 8.

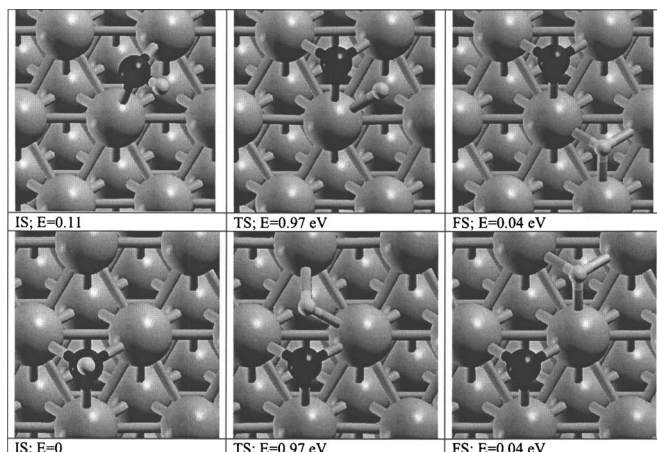


FIG. 7. Initial state (IS), transition state (TS), and final state (FS) of two possible MEPS for the $\text{OH} \rightarrow \text{O} + \text{H}$ reaction on Ni(111). NEB calculations were performed using five images.

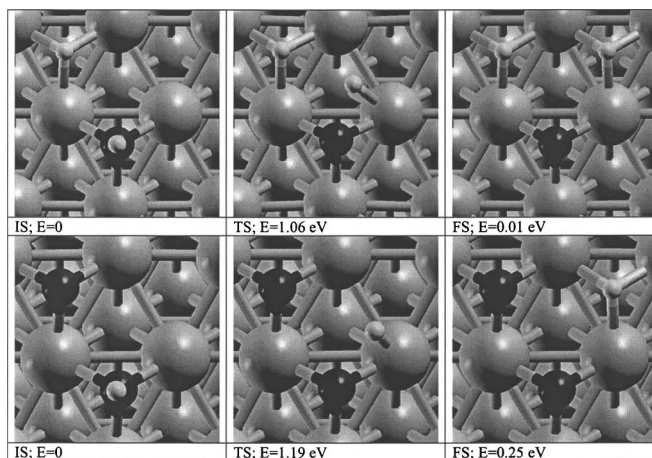


FIG. 8. As in Fig. 7 but in the presence of a coadsorbed H atom (top panels) or O atom (bottom panels) as “spectators.” NEB calculations were performed using seven images.

For the water molecule, we find an activation energy for the dissociation into H and OH of 0.89 eV, which is somewhat less than 0.92 eV found on the Rh surface. We show in Fig. 9 the IS, TS, and FS for comparison with the Rh(111) case. The calculations were performed using seven images. We observe that the transition state is somewhat different in this case, with the H atom sitting essentially in its final state hollow site already rather than in the bridgelike site found on Rh(111). The activation energies for the formation of OH first, followed by the formation of the water molecule from OH and H, are 1.30 and 1.05 eV on Ni, to be compared with the values of 1.10 and 0.82 eV on the Rh surface. This implies that the formation of water on Ni is more difficult than on Rh, making Ni, in this respect, a better catalytic substitute to Pt than Rh for catalytic partial oxidation of methane.

J. Dependence of the results on unit cell size and Rh bulk lattice parameter

In order to test the adequacy of the 2×2 unit cell, and also the robustness of the results on the exact choice of lattice parameter, we have repeated some of the calculations presented for Rh(111) in the previous sections using a 3×3 surface unit cell.

In Table VI we report the adsorption energies for the O and H atoms and the OH and H₂O molecules calculated using a 3×3 unit cell, and also (in parentheses) the values obtained using a lattice parameter of 3.86 Å. If we compare these results with those obtained using the 2×2 unit cell we see that differences are extremely small. We also notice that

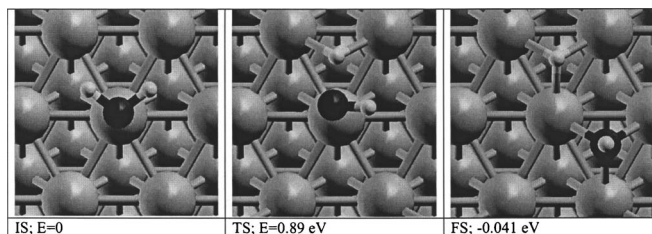


FIG. 9. IS, TS, and FS for the reaction $\text{H}_2\text{O} \rightarrow \text{OH} + \text{H}$ on Ni(111). NEB calculations were performed using seven images.

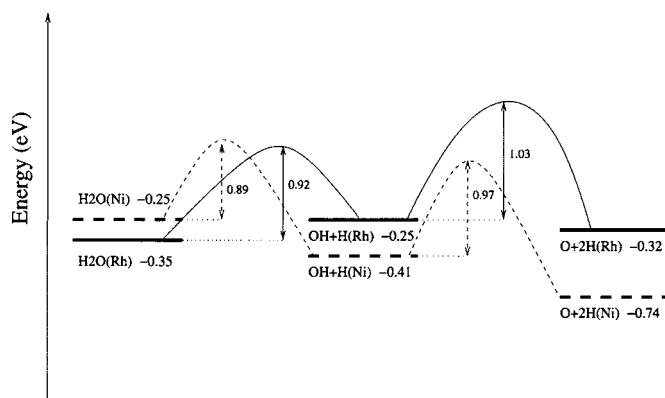


FIG. 10. Energy diagram for the dissociation/formation barriers of OH and H_2O on Rh(111) and Ni(111) as summarized in Tables VII and VIII. Solid and dashed lines correspond to calculations on Rh(111) and Ni(111), respectively. Energy points are not in scale.

the exact value of the lattice parameter (3.81 or 3.86 Å) does not affect significantly the calculated adsorption energies, with differences of only 0.03–0.04 eV for a 1.3% change in lattice parameter, consistent with the findings of Mavrikakis *et al.*⁵⁷ who found a change of slightly over 0.05 eV in the adsorption energy of O on Ru(0001) for a relative change in surface lattice constant of 1.3%.

We have also tested the effect of the size of the cell on the evaluation of the energy barriers for the dissociation of the OH and the H_2O molecules. By repeating the calculations using the 3×3 unit cell, we find that the activation energy for the dissociation of the OH molecule is 1.00 eV, only marginally lower than the value of 1.03 eV found with the 2×2 unit cell. The energy difference between the transition state and the isolated atoms on the surface is 1.11 eV, which is identical to that obtained with the 2×2 unit cell.

We have repeated some calculations also with the lattice parameter of 3.86 Å for the 3×3 cell and found for the two barriers the values of 1.02 and 1.13 eV, which are further confirmation that the exact value of the lattice parameter is affecting only marginally the calculated activation energies.

We repeated the calculation of the dissociation of the OH molecule in the presence of a coadsorbed O atom, and in this case we found that the energy barrier is reduced from 1.37 to 1.13 eV as the coverage is reduced from 0.25 to 0.11 ML. This is the only case where we have noticed a significant size effect in the calculated properties. It is interesting to notice that the value of the energy barrier at low coverage (1.13 eV) is closer to that obtained with the isolated OH molecule, pointing to a reduction of the catalytic activity of the surface due to the presence of extra oxygen.

Finally, we have also repeated the calculations of the activation energy for the dissociation of the water molecule using a 3×3 unit cell and the lattice parameter of 3.86 Å. We found that the activation energy is 0.94 eV, essentially the same as that obtained using the 2×2 unit cell and the lattice parameter of 3.81 Å.

K. Energy diagrams

The water formation/dissociation reaction energy diagrams on Rh(111) and on Ni(111) are shown in Fig. 10.

TABLE VII. Energy diagram for reactions on Rh(111). Values of binding energies of gas (*g*) and adsorbates (*a*) and energy barriers have been calculated using a 2×2 unit cell. (*) The values of the energy barrier obtained respectively with a coadsorbed H or O atom as “spectators” are instead 1.11 and 1.37 eV.

	Energy (eV)	Energy barrier to next step (eV)
$\text{O}_g + \text{H}_g + \text{H}_g + \text{Rh}(111)$	0.0	
$\text{OH}_g + \text{H}_g + \text{Rh}(111)$	-4.81	
$\text{H}_2\text{O}_g + \text{Rh}(111)$	-10.32	
$\text{H}_2\text{O}_a + \text{Rh}(111)$	-10.67	0.92
$\text{OH}_a + \text{H}_a + \text{Rh}(111)$	-10.57	1.03*
$\text{O}_a + \text{H}_a + \text{H}_a + \text{Rh}(111)$	-10.64	
$1/2\text{O}_2_g + \text{H}_2_g + \text{Rh}(111)$	-7.83	

Tables VII and VIII summarize, for completeness, the overall numerical values of the reaction, starting from atomic oxygen and hydrogen in the gas phase plus the clean Rh(111) or Ni(111) surface, followed by OH plus atomic hydrogen, proceeding through the formation of the water molecule (still in the gas phase), its adsorption on the surface, its dissociation into the adsorbate products OH and H and subsequently into atomic O and H atoms, and finally leading to desorption of molecular oxygen and molecular hydrogen.

IV. CONCLUSIONS

In this comparison study we have investigated the dissociation and formation of water on the Rh(111) and Ni(111) metal surfaces using *ab initio* density functional theory calculations.

On both Rh(111) and Ni(111) surfaces water adsorbs flat on a top site, with binding energies of 0.35 and 0.25 eV, respectively. We also find that on both surfaces, the water molecule is free to rotate in the surface plane. The activation energies for its dissociation into OH and H are of 0.92 eV on Rh(111) and 0.89 eV on Ni(111) metal surfaces, while further 1.03 and 0.97 eV are needed, respectively, to dissociate OH into O and H. The activation energies for the formation of the hydroxyl molecule OH from its isolated adsorbates O and H are found to be 1.1 and 1.3 eV, while those for the

TABLE VIII. Energy diagram for reactions on Ni(111). Values of binding energies of gas (*g*) and adsorbates (*a*) and energy barriers have been calculated using a 2×2 unit cell. The value of the energy barrier in parentheses has been obtained with a non-spin-polarized calculation. (*) The values of the energy barrier obtained respectively with a coadsorbed H or O atom as “spectators” are instead 1.06 and 1.19 eV.

	Energy (eV)	Energy barrier to next step (eV)
$\text{O}_g + \text{H}_g + \text{H}_g + \text{Ni}(111)$	0.0	
$\text{OH}_g + \text{H}_g + \text{Ni}(111)$	-4.81	
$\text{H}_2\text{O}_g + \text{Ni}(111)$	-10.32	
$\text{H}_2\text{O}_a + \text{Ni}(111)$	-10.57	0.89 (0.70)
$\text{OH}_a + \text{H}_a + \text{Ni}(111)$	-10.73	0.97*
$\text{O}_a + \text{H}_a + \text{H}_a + \text{Ni}(111)$	-11.06	
$1/2\text{O}_2_g + \text{H}_2_g + \text{Ni}(111)$	-7.83	

formation of the water molecule from its isolated adsorbates OH and H are 0.82 and 1.05 eV on Rh(111) and Ni(111), respectively.

The dissociation energy of OH has also been studied by coadsorbing a H or O atom on the surface. Not surprisingly, we found that the presence of coadsorbed species and O, in particular, significantly affects the values of the dissociation energy barriers, which on Rh(111) go from 1.03 to 1.11 and 1.37 eV with coadsorbed H and O, respectively, at 0.25 ML coverage, and on Ni(111) from 0.97 to 1.06 and 1.19 eV, respectively. This is expected, due to the surface reactivity reduction caused by the presence of adsorbates and, in particular, oxygen. As coverage is reduced from 0.25 to 0.11 ML the effect of the presence of coadsorbed O on the height of the energy barrier for the dissociation of OH is greatly reduced, with a calculated barrier of 1.13 eV on Rh(111), which is much closer to those obtained when the OH molecule is isolated on the surface.

For water dissociation, we also studied a reaction path on Rh(111) which involved an extra O atom coadsorbed on the surface, with the water molecule donating a proton to this O to form OH+OH. For this reaction we found that the energy barrier needed to be overcome in order to dissociate the water molecule into two hydroxyl molecules is only of 0.56 eV.

For both Rh(111) and Ni(111) surfaces, we find that the binding energies are ordered as $H < OH < O$ (where O is the most strongly bound). The activation energy for the dissociation of OH into O and H is about 6% lower on Ni than on Rh, implying that the process is slightly more easier on Ni than on Rh surfaces. Conversely, the activation energy for OH formation from its dissociation products is about 15% higher for Ni than for Rh.

We also found that the activation barrier for water dissociation on Ni(111) is about 3% higher than on Rh(111), and the activation energy for water formation from its dissociation products is over 20% higher on Ni than on Rh. More importantly, we find that the adsorption energy of the water molecule on the Rh(111) surface is roughly equal to the adsorption energy of its dissociation products, the oxygen atom and two hydrogen atoms, but on Ni(111) these dissociation products have an adsorption energy which is almost 0.5 eV lower than that of the water molecule, making the dissociation of the molecule thermodynamically advantageous. This has important implications for the design of catalysts to be employed in reactions involving the production/dissociation of water.

ACKNOWLEDGMENTS

This work was conducted as part of a EURYI scheme award as provided by EPSRC (see www.esf.org/euryi) and partially funded by Integra Srl. Allocation of computer time has been provided by UCL research computing and Integra Srl. The authors thank A. Suriano and S. Baroni for useful discussions.

¹P. A. Thiel and T. E. Madey, Surf. Sci. Rep. **7**, 211 (1987).

²M. A. Henderson, Surf. Sci. Rep. **46**, 1 (2002).

³H. Yang and J. L. Whitten, Surf. Sci. **223**, 131 (1989).

⁴A. Michaelides, Appl. Phys. A **85**, 415 (2006).

⁵D. A. Hickman and L. D. Schmidt, Science **259**, 343 (1993).

⁶J. T. Keiser, M. A. Hoffbauer, and M. C. Lin, J. Phys. Chem. **89**, 2635 (1985).

⁷M.-S. Liao, C.-T. Au, and C.-F. Ng, Chem. Phys. Lett. **272**, 445 (1997).

⁸Y. Morikawa, J. J. Mortensen, B. Hammer, and J. K. Nørskov, Surf. Sci. **386**, 67 (1997).

⁹W.-S. Dong, H.-S. Roh, Z.-W. Liu, K.-W. Jun, and S.-E. Park, Bull. Korean Chem. Soc. **22**, 1323 (2001).

¹⁰L. Schlapbach and A. Züttel, Nature (London) **414**, 353 (2001).

¹¹A. Züttel, Naturwiss. **91**, 157 (2004).

¹²S. Wilke, V. Natoli, and H. Cohen, J. Chem. Phys. **112**, 9986 (2000).

¹³S. Meng, E. G. Wang, and S. Gao, Phys. Rev. B **69**, 195404 (2004).

¹⁴A. Michaelides, V. A. Ranea, P. L. de Andres, and D. A. King, Phys. Rev. Lett. **90**, 216102 (2003).

¹⁵G. S. Karlberg, Phys. Rev. B **74**, 153414 (2006).

¹⁶K. Christmann, Surf. Sci. Rep. **9**, 1 (1988); Mol. Phys. **66**, 1 (1989); Prog. Surf. Sci. **48**, 15 (1995).

¹⁷J. Greeley and M. Mavrikakis, J. Phys. Chem. B **109**, 3460 (2005).

¹⁸M. Mavrikakis, J. Rempel, J. Greeley, L. B. Hansen, and J. K. Nørskov, J. Chem. Phys. **117**, 6737 (2002).

¹⁹H. Yang and J. L. Whitten, J. Chem. Phys. **98**, 5039 (1993).

²⁰J.-F. Paul and P. Sautet, Surf. Sci. **356**, L403 (1996).

²¹G. Kresse and J. Hafner, Surf. Sci. **459**, 287 (2000).

²²A. Michaelides and P. Hu, J. Chem. Phys. **112**, 6006 (2000).

²³M. V. Ganduglia-Pirovano and M. Scheffler, Phys. Rev. B **59**, 15533 (1999).

²⁴H. Yang and J. L. Whitten, Surf. Sci. **370**, 136 (1997).

²⁵T. W. Root, L. D. Schmidt, and G. B. Fisher, Surf. Sci. **134**, 30 (1983).

²⁶M. L. Wagner and L. D. Schmidt, J. Phys. Chem. **99**, 805 (1995).

²⁷M. P. Zum Mallen, W. R. Williams, and L. D. Schmidt, J. Phys. Chem. **97**, 625 (1993).

²⁸J. P. Perdew, K. Burke, and M. Ernzerhof, Phys. Rev. Lett. **77**, 3865 (1996).

²⁹D. Vanderbilt, Phys. Rev. B **41**, 7892 (1990).

³⁰S. Baroni, A. Dal Corso, S. de Gironcoli, and P. Giannozzi, <http://www.pwscf.org>

³¹A. Kokalj, Comput. Mater. Sci. **28**, 155 (2003); <http://www.xcrysden.org/>

³²M. Methfessel and A. Paxton, Phys. Rev. B **40**, 3616 (1989).

³³G. Mills, H. Jonsson, and G. K. Schenter, Surf. Sci. **324**, 305 (1995); H. Jonsson, G. Mills, and K. W. Jakobsen, in *Classical and Quantum Dynamics in Condensed Phase Simulations*, edited by B. J. Berne, G. Cicotti, and D. F. Coker (World Scientific, Singapore, 1998); G. Henkelman and H. Jonsson, J. Chem. Phys. **113**, 9978 (2000); G. Henkelman, B. P. Uberuaga, and H. Jonsson, *ibid.* **113**, 9901 (2000); the NEB method has been implemented in the pwscf code by Carlo Sbraccia.

³⁴F. Birch, Phys. Rev. **71**, 809 (1947).

³⁵*CRC Handbook of Chemistry and Physics*, 83rd ed., edited by D. R. Lide (CRC, New York, 2002).

³⁶C. Kittel, *Introduction to Solid State Physics*, 7th ed. (Wiley, New York, 1996).

³⁷F. Mittendorfer, A. Eichler, and J. Hafner, Surf. Sci. **423**, 1 (1999).

³⁸H. C. Lu, E. P. Gusev, E. Garfunkel, and T. Gustafsson, Surf. Sci. **352**, 21 (1996).

³⁹B. H. Bransden and C. J. Joachin, *Physics of Atoms and Molecules* (Wiley, New York, 1983).

⁴⁰K. Huber and G. Herzberg, *Constants of Diatomic Molecules*, Molecular Spectra and Molecular Structure Vol. 4 (Van Nostrand, Princeton, 1979).

⁴¹D. C. Patton, D. V. Porezag, and M. R. Pederson, Phys. Rev. B **75**, 7454 (1997).

⁴²J. A. Pople, M. Head-Gordon, D. J. Fox, K. Raghavachari, and L. A. Curtiss, J. Chem. Phys. **90**, 5622 (1989).

⁴³W. S. Benedict, N. Gailar, and E. K. Plyler, J. Chem. Phys. **24**, 1139 (1956).

⁴⁴M. Sprick, J. Hutter, and M. Parrinello, J. Chem. Phys. **105**, 1142 (1996).

⁴⁵S. Schwegemann, H. Over, V. de Renzi, and G. Ertl, Surf. Sci. **375**, 91 (1997).

⁴⁶D. T. Vu Grimsby, Y. K. Wu, and K. A. R. Mitchell, Surf. Sci. **232**, 51 (1990).

⁴⁷L. Hammer, H. Landskron, H. Nichtl-Pecher, A. Fricke, K. Heinz, and K. Müller, Phys. Rev. B **47**, 15969 (1993).

⁴⁸J. J. Zinck and W. H. Weinberg, J. Vac. Sci. Technol. **17**, 188 (1980).

- ⁴⁹J.-S. Lin, A. Qteish, M. C. Payne, and V. Heine, *Phys. Rev. B* **47**, 4174 (1993).
- ⁵⁰K. Christmann, R. J. Behm, G. Ertl, M. A. Van Hove, and W. H. Weinberg, *J. Chem. Phys.* **70**, 4168 (1979).
- ⁵¹T. E. Madey and F. P. Netzer, *Surf. Sci.* **117**, 549 (1982).
- ⁵²R. H. Stulen and P. A. Thiel, *Surf. Sci.* **157**, 99 (1985).
- ⁵³D. Alfè and M. Gillan, *J. Phys.: Condens. Matter* **18**, L451 (2006).
- ⁵⁴P. A. Thiel, J. T. Yates, Jr., and W. H. Weinberg, *Surf. Sci.* **82**, 22 (1979).
- ⁵⁵S. S. Mann, T. Seto, C. J. Barnes, and D. A. King, *Surf. Sci.* **261**, 155 (1992).
- ⁵⁶G. X. Cao, E. Nabighian, and X. D. Zhu, *Phys. Rev. Lett.* **79**, 3696 (1997).
- ⁵⁷M. Mavrikakis, B. Hammer, and J. K. Nørskov, *Phys. Rev. Lett.* **81**, 2819 (1998).